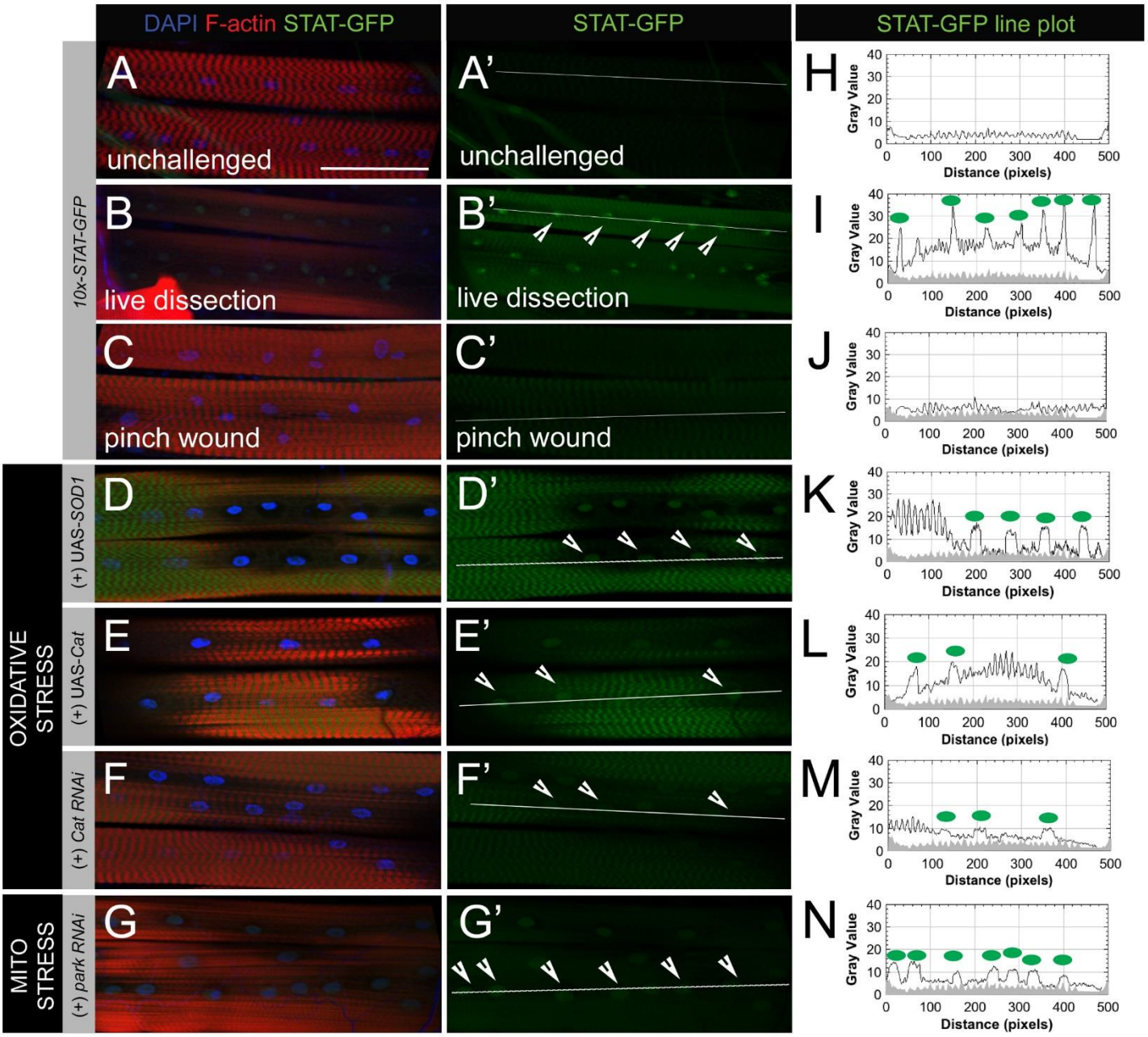

Figure S1. Additional muscle stressors initiating JAK/STAT signaling in larval muscle. (A-G) Muscle morphology (F-actin; red) of an L3 ventral longitudinal (VL) muscle pair (m. 6,7) merged with nuclear staining (DAPI; blue) and STAT-GFP (GFP; green) reporter expression. (A'-G') STAT-GFP reporter expression (green) in muscles with either physical injury (B'-C') or (D'-G') genetic manipulations applied. (B,B') Muscle damage sustained during live dissection of muscle fillets triggers a dramatic increase in STAT-GFP expression. All other larvae were heat killed prior to dissection to mitigate this effect. (C,C') At two hours post pinch wound, STAT-GFP expression is only slightly elevated compared to that of unchallenged individuals (A'). Alterations to oxidative balance through either the overexpression of *SOD1* (D,D'), *Cat* (E,E'), or the knockdown of *Cat* via

RNAi (F,F') activates JAK-STAT signaling. (G,G') Reduction of *park* transcripts through RNAi causes mitochondrial stress and initiates low, but detectable increases in STAT-GFP expression. (H-N) Line plot of STAT-GFP intensity along a representative L3 VL muscle (white line). GFP intensity from *STAT-GFP* control muscle in panel H is overlaid on line plots as a grey-filled profile in panels I-N. Regions of staining corresponding to nuclear expression are indicated by green ovals on plot and correspond to arrowheads in panels A'-G' for reference. Scale bars 100 μm for A-G'.

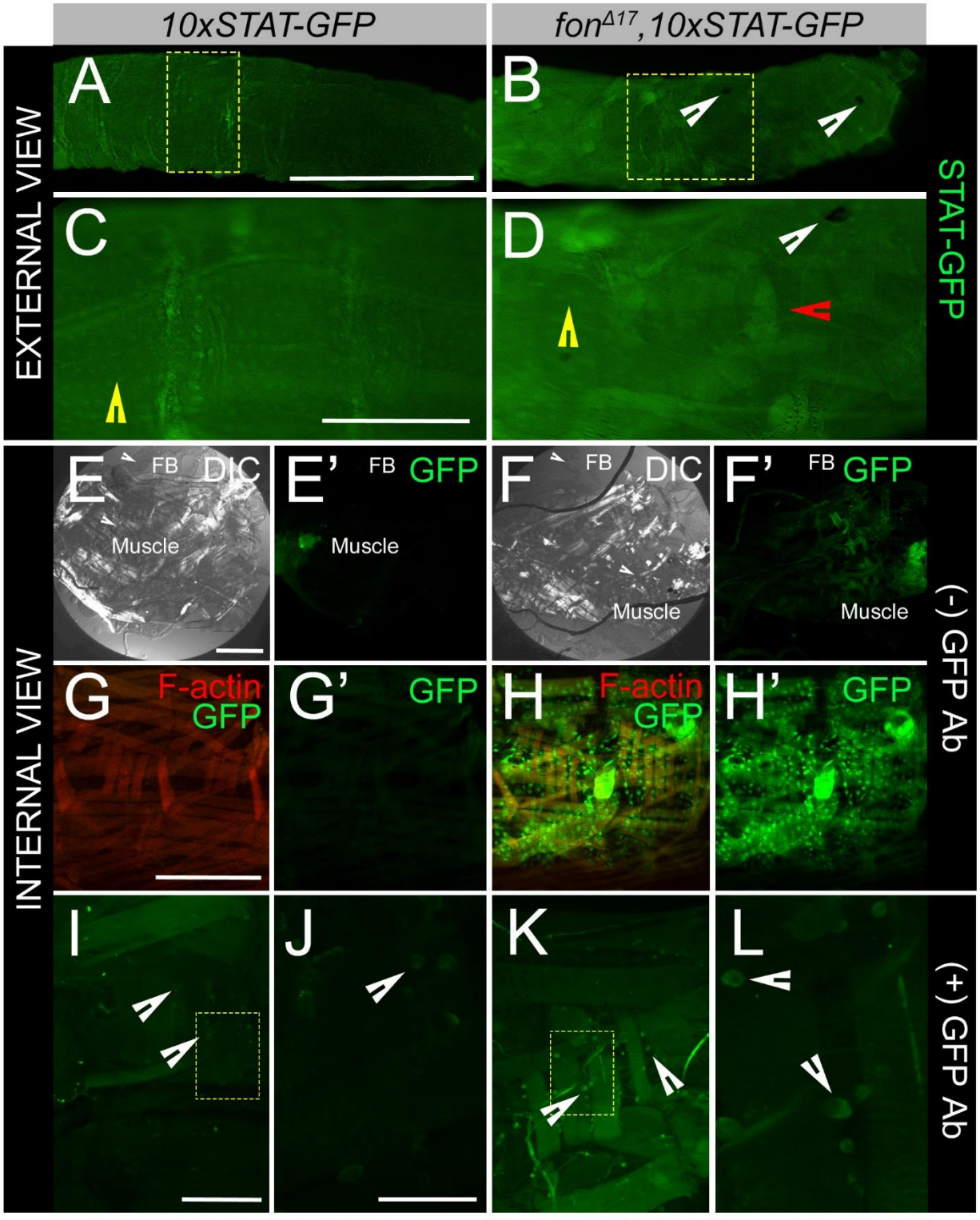

Figure S2. Tissue localization of 10xSTAT-GFP reporter in *fon* mutant larvae. (A-D) External views of *STAT-GFP* reporter in L3 larvae free of muscle damage (A,C) or containing detached muscles from loss of *fon* (B,D). Higher magnification images (C,D) taken of regions (yellow box) indicated in panels A and B. (A,C) Basal STAT-

GFP expression can be seen in the cuticle and epithelial cells (yellow arrowhead) of unstressed larvae. (B,D) Loss of *fon* causes muscle detachment and increases to JAK/STAT signaling in muscle tissue (red arrowhead), as well as expression in the cuticle and epithelial cells (yellow arrowhead). The presence of melanotic tumors in *fon* mutants is marked with white arrowheads. (E-H') Internal views of STAT-GFP expression in larval tissues at high and low magnification. (E-F') Broad view of tissues in L3 larvae positioned anterior (left) to posterior (right). STAT-GFP is relatively absent from larval fillets with all internal tissues left intact, notably the fat body (FB) and muscle which are indicated by arrowheads on the DIC image (E). Loss of *fon* causes STAT-GFP to increase in muscle, but not fat body (FB) tissue which are labeled in DIC images by arrowheads. (G-H') Internal views of the increase in STAT-GFP in both muscle and epithelial tissues in *fon* mutants (H,H') compared to control larvae (G,G') recapitulate the expression patterns seen in external images (A-D). (I-L) STAT-GFP expression in hemocytes enhanced by GFP antibody. Hemocytes in both *WT* and *fon* mutants (arrowheads) express STAT-GFP. Panels J and L are higher magnification images of hemocytes outlined in yellow boxes (I,K). Scale bars 1 mm A-B, C-D, 500 μm C-H', 250 μm I,K, 50 μm J,L.

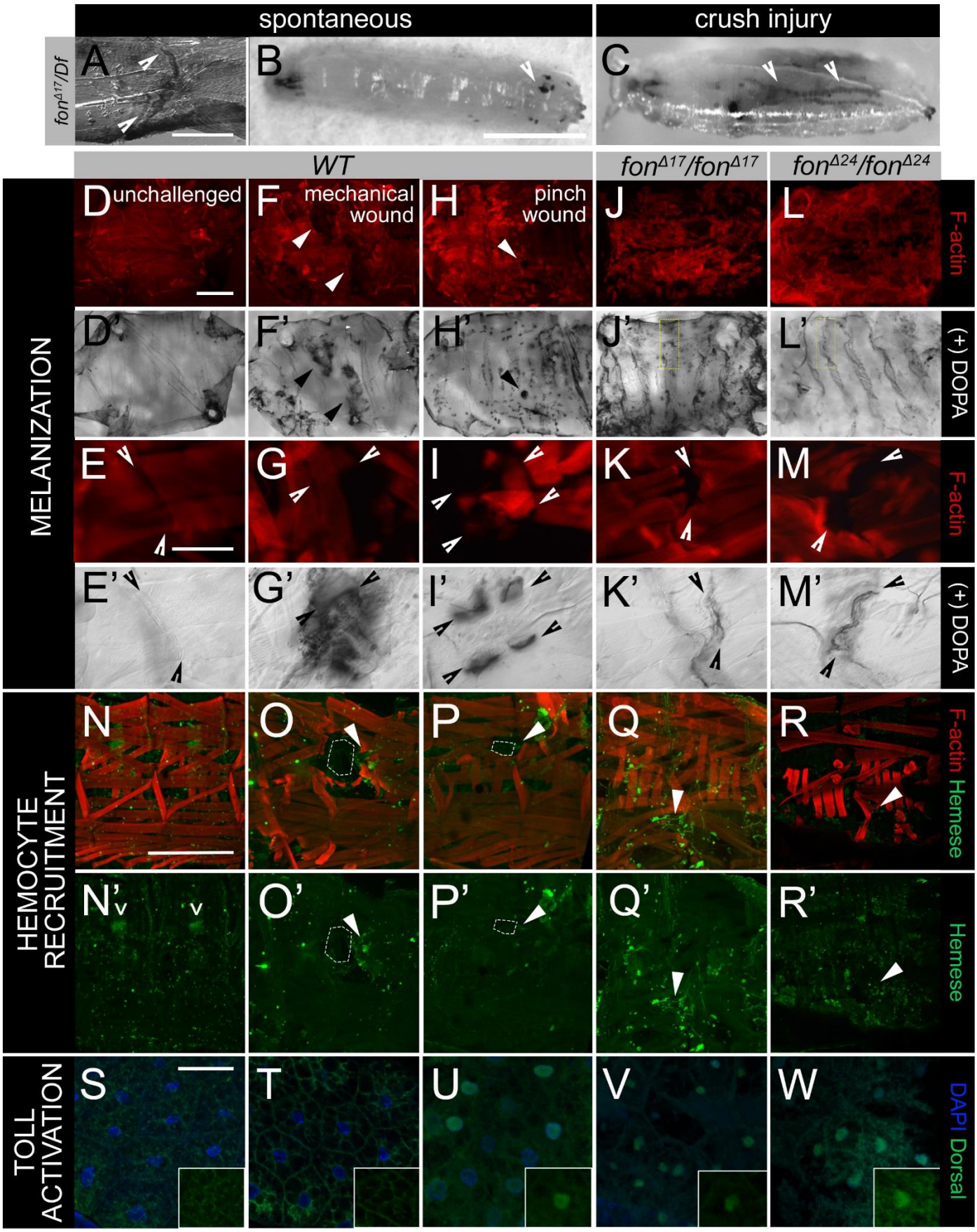
spontaneous
crush injury
fon^Δ17/Df
A
B
C
WT
fon^Δ17/fon^Δ17
fon^Δ24/fon^Δ24
MELANIZATION
D unchallenged
F mechanical wound
H pinch wound
J
L
F-actin
D'
F'
H'
J'
L'
(+) DOPA
E
G
I
K
M
F-actin
E'
G'
I'
K'
M'
(+) DOPA
HEMOCYTE RECRUITMENT
N
O
P
Q
R
F-actin Hemese
N'v
v
O'
P'
Q'
R'
Hemese
TOLL ACTIVATION
S
T
U
V
W
DAPI Dorsal

Figure S3. Characterization of immune responses induced by various muscle stresses. (A-C) Additional melanization phenotypes of *fon*$^{\Delta 17}$ homozygotes induced spontaneously (A-B) or through external trauma (C). (A) Accumulation of melanin at a MAS where melanization has been spontaneously induced upon loss of *fon*. (B) Melanin also forms melanotic tumors within the body cavity of *fon* mutants which may by free in the hemolymph or adhere to tissues. (C) Melanin collects along the pericardial cells of the dorsal vessel (arrowheads) following a crush injury to a *fon* mutant larvae which has begun to pupate. (D-M') Muscle morphology (F-actin; red) of dissected L3 larval fillets which have been dissected in the PO substrate, DOPA, and imaged by DIC for the presence of melanization (black). Muscle damage caused by trauma-based injury (site of injury indicated by solid arrows in F-H') or in genetic backgrounds with muscle detachment (J-M') experience melanization near MASs (arrowheads) or the ends of damaged muscles as compared to uninjured *WT* muscle fillets which are free of melanin except for areas along the cuticle (D-E'). (N-R') Recruitment of hemocytes (Hemese; green) within muscle hemisegments (F-actin; red) during muscle damage. In *WT* fillets without tissue damage, a population of sessile hemocytes (white caret) is distributed between the muscle and epithelial layer (N-N'). Upon muscle damage induced by forceps (O-O'; white dotted outline), hemocytes are strongly recruited to damaged muscles and adhere in clusters (solid arrowhead). (P-P') Damage induced through pinch wounding (white dotted outline) is less disruptive to muscle tissue and subsequently target hemocytes at very low levels (solid arrowheads). (Q-R') Detached muscles in *fon* mutants are decorated with hemocytes recruited from the hemolymph. (S-W) Dl (green) subcellular localization in fat bodies of larvae. A single fat body cell is pictured in insets within each panel. In larvae with muscles 4 hours post-pinch wound (P) or muscle detachment (Q,R), Toll signaling is active in fat bodies and Dl concentrates in the nucleus. Scale bars 100 μm A,E,E',G,G',I,I',K,K',M,M', 1 mm B-C, 500 μm D,D',F,F',H,H',J,J',L,L', N-R', 50 μm S-W'.

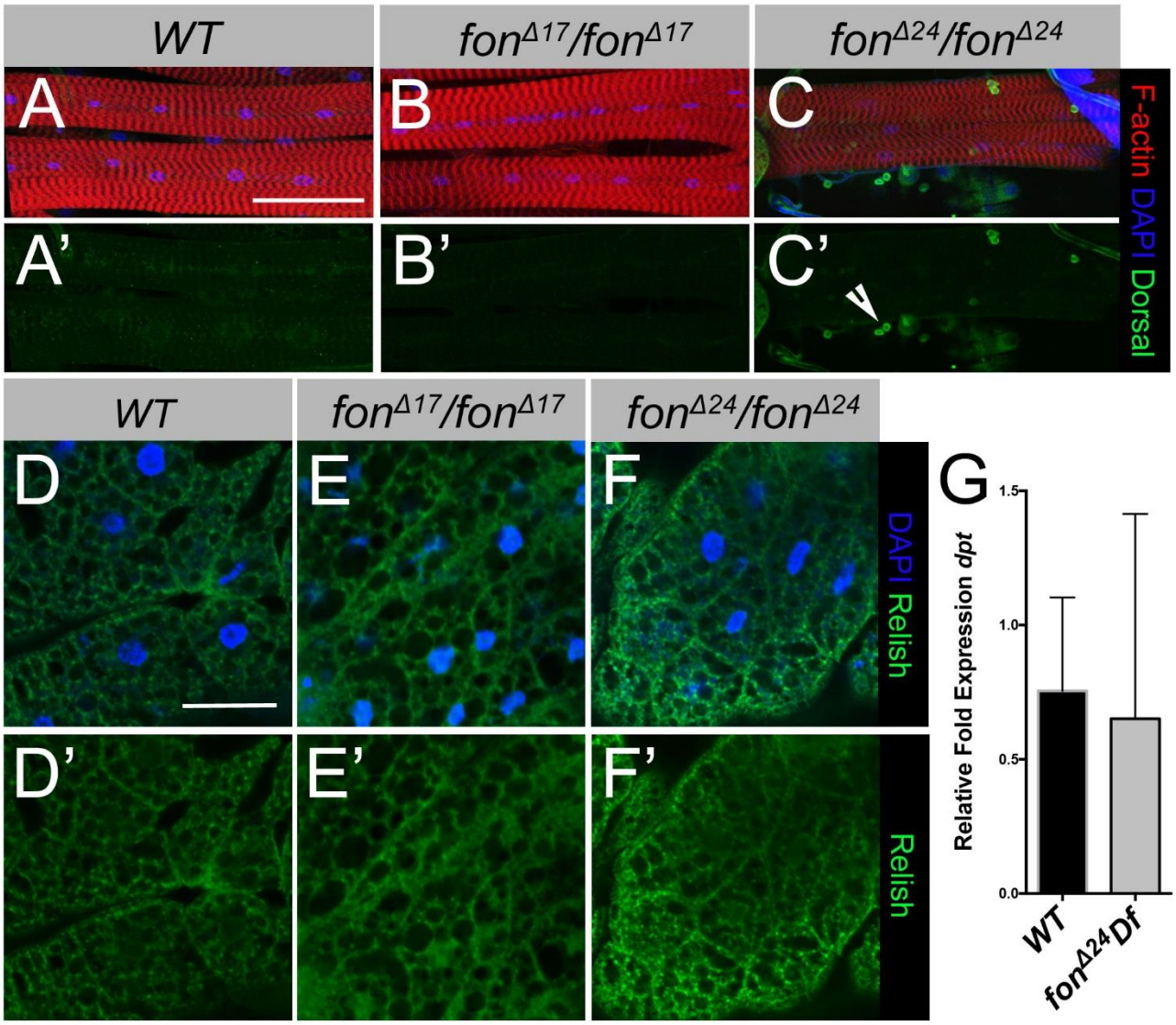

Figure S4. NF-κB signaling unchanged by loss *of fon*. (A-B') Dl expression (green) in L3 ventral longitudinal muscles (F-actin; red) of *WT* and *fon* mutants. (A,A') Dl is faintly detected in *WT* larval muscles with stable MASs. (B-C') Localization of Dl within detached muscles is difficult to detect. However, in muscles that remain attached in $fon^{\Delta 17}$ (B-B') or $fon^{\Delta 24}$ (C,C') homozygotes increasing levels of Dl in either the cytoplasm or nucleus of muscle tissue is not observed. Hemocytes positioned near muscle of *fon* mutants (C', arrowheads) contain Dorsal staining, although it is restricted to the cytoplasm. (D-F') Subcellular localization of Relish (Rel) within larval fat body cells. Similar to activation of Toll signaling, signal transduction through the Imd pathway causes the transcription factor, Rel, to move into the nucleus. In *WT* (D,D'), $fon^{\Delta 17}$ (E,E'), and $fon^{\Delta 24}$ (F,F') larvae, Rel staining is found in the cytoplasm. (G) *Dpt* expression levels in isolated $fon^{\Delta 24}$ fat bodies remain similar to transcript levels in unchallenged *WT* fat bodies. Mean ± SD. Scale bars 100 μm for A-C', 50 μm D-F'.

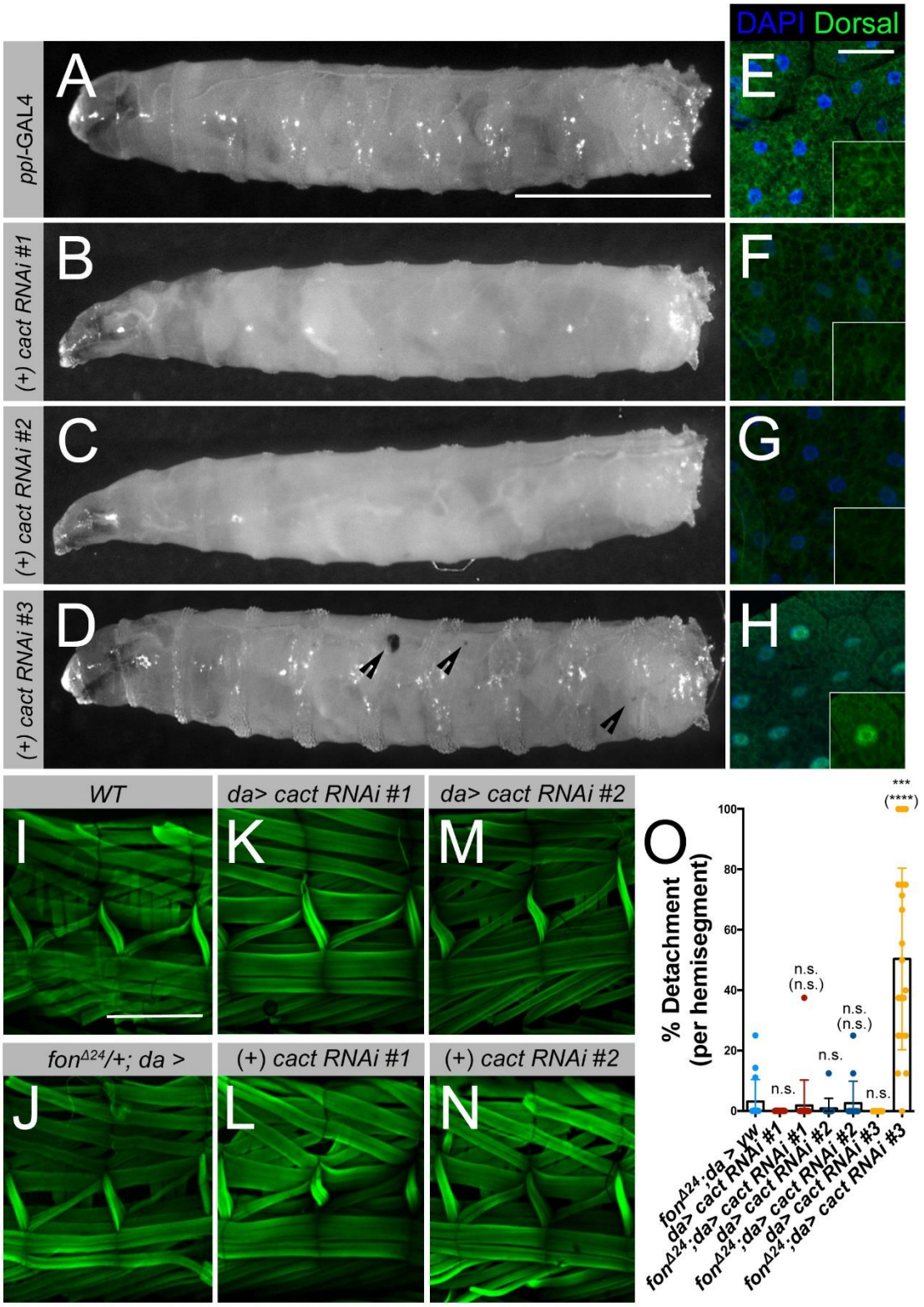

Figure S5. Validation of *cact RNAi* lines. (A-D) External view of wandering L3 larvae of the specified genotypes. In *ppl*-GAL4 larvae unchallenged by pathogens, the body cavity is free of melanization (A). Bloomington TRiP *cact* RNAi stocks #1 (B) and #2 (C) fail to produce melanotic nodules similar to reported

phenotypes in *cact* mutants (see Materials and Methods for corresponding BL stock identifiers). Only RNAi knockdown using *cact RNAi* #3 in the fat body was sufficient to produce melanotic tumors (D, black arrowheads). (E-H) Dl (green) localization within fat bodies following RNAi knockdown of *cact.* Insets depict Dl staining without DAPI in a single fat body cell. Under normal conditions, Dl is sequestered in the cytoplasm of fat body cells by the presence of Cact (E). RNAi knockdown using *cact RNAi #1* and *#2* have Dl localizations similar to *WT* fat body cells (F-G). Consistent with the induction of melanotic tumors, only RNAi knockdown using *cact RNAi #3* occurs at levels necessary for the translocation of Dl into the fat body nucleus (H). (I-N) Sensitized background screen for muscle detachment caused by *cact* RNAi knockdown using available TRiP RNAi stocks. Unlike *cact RNAi #3*, knockdown of cact using *cact RNAi #1* and *cact RNAi #2* does not cause muscle detachment independently or in combination with loss of a single copy of *fon* (compare to Figure 5). (O) Quantification of muscle detachment upon RNAi knockdown using *cact RNAi* stocks either alone or in a *fon*-sensitized background (*fon$^{\Delta 24}$; da>w1118,* n=16; *da> cact RNAi #1,* n=20; *fon$^{\Delta 24}$; da> cact RNAi #1,* n=20; *da> cact RNAi #2,* n=14; *fon$^{\Delta 24}$; da> cact RNAi #2,* n=14; *da> cact RNAi #3,* n=16; *fon$^{\Delta 24}$; da> cact RNAi #3,* n=21). Mean ± SD; *P*-values determined via Kruskal-Wallis statistical test: *** *P* <.001, **** *P* <.0001, n.s., not significant. *P*-values for comparisons to the sensitized background (*fon$^{\Delta 24}$; da>* +) alone are placed above each RNAi line. *P*-values of comparisons between RNAi alone and in combination with the sensitized background are denoted in parentheses. Scale bars 1 mm A-D, 50 μm E-H, 500 μm I-N.

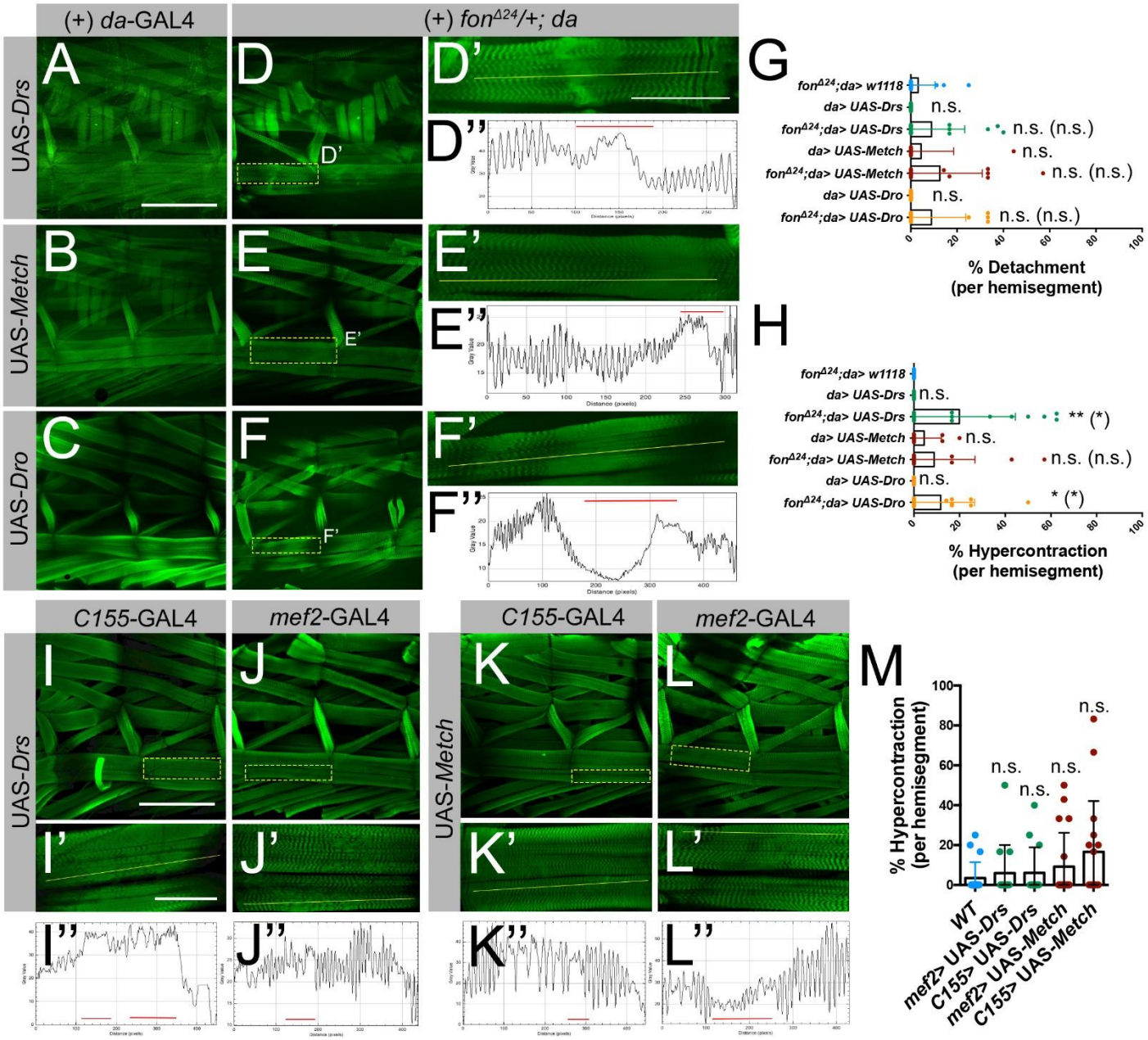

Figure S6. Overexpression of AMPs disrupts muscle maintenance. (A-C) Muscle morphology in two hemisgements of L3 muscle fillets (F-actin; green) following AMP overexpression. Overexpression of AMPs in a *fon*-sensitized genetic background at low magnification (D-F) and high magnification with line plot analysis (D'-F''). (A-C) Muscle tissue subjected to overexpression of Drs, Metch, and Dro display no visible morphological defects. (D-F) Low magnification images of UAS-*AMP* overexpression in the *fon*-sensitized background. (D'-F') High magnification images of boxed muscles (yellow box) following AMP overexpression of *Drs*, *metch*, and *Dro* in a *fon*-sensitized background. Compared to AMP overexpression alone, the combination of one copy of *fon* and heightened levels of *Drs, metch,* and, *Dro* cause an increasing trend of muscle detachment (G) and

significant levels of hypercontraction (D'-F', H). (D''-F'') Representative line plot analysis of F-actin sarcomeric staining across a single ventral lateral L3 muscle (yellow line). Regions of compressed sarcomeres are indicated by red lines on individual line plots. (G, H) Quantification of muscle detachment (G) and hypercontraction (H) in indicated genotypes *(fon$^{\Delta 24}$; da>* yw, n=16; *da> UAS-Drs,* n=13; *fon$^{\Delta 24}$; da> UAS-Drs,* n=18; *da>UAS-Metch,* n=10; *fon$^{\Delta 24}$; da> UAS-Metch,* n=15; *da>UAS-Dro,* n=15; *fon$^{\Delta 24}$; da> UAS-Dro,* n=14). (I-L) Muscle morphology of two L3 muscle hemisegments with AMP expression driven in either neural (*C155*-GAL4) or muscle (*mef2*-GAL4) tissue. (I'-L') High magnification images of hypercontracted muscles with tissue-specific expression of Drs (I'-J') or Metch (K'-L'). (I''-L'') Representative line plot analysis of sarcomeres taken along a ventral longitudinal muscle. Hypercontracted regions are indicated by red lines on line plot. (M) Quantification of muscle hypercontraction in tissue-specific AMP overexpression (*WT,* n=18; *C155> UAS-Drs,* n=14; *mef2> UAS-Drs,* n=14; *C155> UAS-Metch,* n=16; *mef2> UAS-Metch,* n=19). Mean ± SD; *P*-values determined via Kruskal-Wallis statistical test: * *P* <.05, ** *P* <.005, n.s. not significant. *P*-values for comparisons to the sensitized background (*fon$^{\Delta 24}$; da> w1118*) alone are placed above each RNAi line. *P*-values of comparisons between RNAi alone and in combination with the sensitized background are denoted in parentheses for quantification in G-H. Scale bars 500 μm A-F, I-L; 100 μm D'-F', I'-L'.

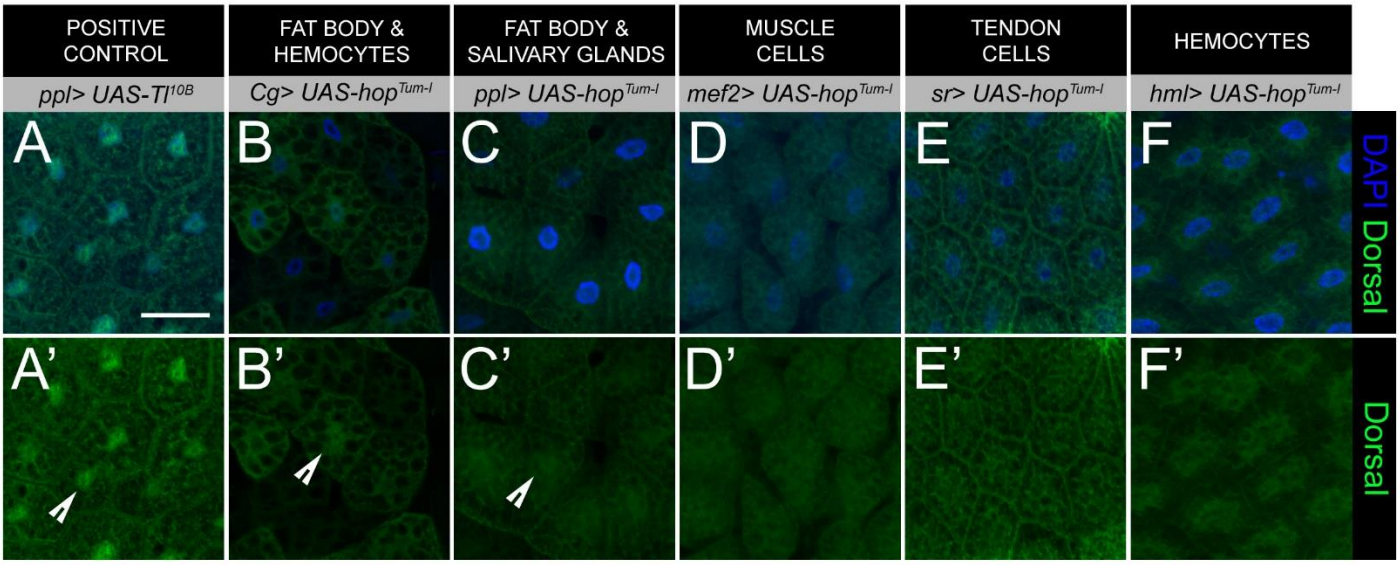

Figure S7. Tissue-specific activation of JAK/STAT signaling is not sufficient to induce systemic Toll signaling. (A,A') Overexpression of a CA Tl receptor in fat body induces translocation of Dl into the nucleus (arrow). The presence of Dl (green) within the fat body nucleus (DAPI; blue) signifies activation of Toll signaling. (B-F') Fat body cells expressing the CA JAK construct, *UAS-hop*$^{tum-l}$ using tissue-specific GAL4 drivers. Expression of CA JAK in fat body tissue using the strong *Cg*-GAL4 driver (B,B') or the weaker *ppl*-GAL4 driver (C,C') causes Dl to weakly translocate to the nucleus (arrows) in the occasional cell, but not in the uniform pattern or intensity observed in the overexpression of CA Tl (A'). Neither expression of CA JAK in the muscle (D,D'), tendon cells (E,E'), or hemocytes (F,F') is capable of inducing active Toll signaling in the fat body. Scale bars 50 μm for A-F'.